Appearance of quasiperiodicity within a period doubling route to chaos of a swaying thermal plume

2014 J. Phys.: Conf. Ser. 501 012022

(http://iopscience.iop.org/1742-6596/501/1/012022)

Journal of Physics: Conference Series **501** (2014) 012022 doi:10.1088/1742-6596/501/1/012022

Appearance of quasiperiodicity within a period doubling route to chaos of a swaying thermal plume

D Angeli[1], M A Corticelli[1], A Fichera[2] and A Pagano [2]

[1] Dipartimento di Ingegneria Enzo Ferrari, Università degli Studi di Modena e Reggio Emilia, Via Vignolese 905, 41125 Modena (Italy)

[2] Dipartimento di Ingegneria Industriale, Università degli Studi di Catania, Viale Andrea Doria 6, 95125 Catania (Italy)

E-mail: [1]diego.angeli@unimore.it

E-mail: [2]apagano@diim.unict.it

Abstract. The birth, evolution and disappearance of quasiperiodic dynamics in buoyancy-driven flow arising from an enclosed horizontal cylinder are analysed here, by numerical means, in the limit of the 2D approximation. The governing equations are solved on orthogonal Cartesian grids, giving special treatment to the internal, non-aligned boundaries. Thanks to the adoption of a high level of refinement of the Rayleigh number range, quasiperiodicity was observed to emerge from a periodic limit cycle (P1), and to turn into its omologous orbit with doubled period (P2), eventually evolving into a classical period-doubling route to chaos, for further increases of the Rayleigh number. The present study gives a deeper insight to what appears to be an imperfect period doubling bifurcation through a quasiperiodic T2-torus. The approach used is based on the classical tools for time series analysis. The distribution of the power spectral densities is used to search for and characterise the existence of relations between the frequencies of the P1, T2 and P2 dynamics. The topology of the orbits, as well as their evolution within the quasiperiodic window, are analysed with the aid of phase space representation and Poincaré maps.

1. Introduction

The strong dependence on the system geometrical configuration and on the thermal boundary conditions is known to determine a great variety of complex buoyancy-driven flows in confined enclosures. In fact, great interest has been given to the non-linear dynamics of thermal convection in basic enclosure configurations, with the heat source either corresponding with the bottom or side walls of the cavity [1, 2]. Several theoretical and experimental studies have also been devoted to the horizontal annulus, as summarized in [3]. For more complex configurations, though most of the effort has been mainly focused on heat transfer performances [4–7], the use of optical techniques such as Particle Image Velocimetry (PIV), has recently allowed the experimental study of the flow field and of its influence on the overall heat transfer[8, 9]. Several authors also dealt with natural convection from enclosed heat sources with the use of state-of-the-art numerical techniques [6, 7, 10–12].

The onset of chaotic dynamics has been addressed in several works. Indeed, the description of the transitional phenomena that drive the dynamics of the flow inside confined cavities, typically from stationary solutions to chaos as the Rayleigh number increases, represents one

of the main research topics in the study of buoyant flows. Different kinds of instabilities and bifurcation scenarios have been reported for different cavity shapes and, for a given shape, for different values of the characteristic aspect ratio. Details of transition vary greatly from one case to another; however, a number of established routes to chaos are found to be common to many types of dissipative dynamical systems [13]. As several types of possible flow regimes are encountered, the simple set of acronyms and abbreviations proposed by Gollub and Benson [14] and extended in [3] is adopted in the following in order to facilitate their description.

With respect to the study of the instabilities and bifurcations of a buoyant plume arising from an enclosed heat source, most of the attention has been devoted to the case of the horizontal annulus. The numerical work of Yoo et al. [15] is of particular interest, although limited to the case of 2D narrow gap annuli (with radius ratio $R = 1.2$) filled with a very low Prandtl number fluid ($Pr = 0.02$). Reported results show that the transition to chaotic flow occurs through the breaking of a quasi-periodic orbit. Later, Yoo and Han [16] investigated the case of a large-gap annulus ($R = 2$), for a slightly larger value of Pr, $Pr = 0.1$, and following an entire route to chaos. The occurrence of a period-tripling bifurcation is observed after the transition to oscillatory flow. The three-period phase (P_3) is interrupted by a window of quasi-periodicity (QP_2); subsequently, a period-doubling cascade (P_6, P_{12}) leads to a first nonperiodic phase (N_I). Before the final transition to chaos (N_{II}), a relaminarisation phase is observed, consisting in a small window of periodicity (P_4) whose frequency is related with the fundamental frequency of the first periodic regime by a factor 4. A very thorough experimental analysis of the transition to chaos in an air-filled annulus with $R = 2.36$ was provided by Labonia and Guj [17]. Quantitative and qualitative measurements were performed by interferometry, smoke visualization and hot wire anemometry. The route to chaos appears to be characterised by a sequence of Hopf transitions, separated by windows of quasiperiodic behaviour.

With respect to other type of cavities with internal heat sources, considerable attention has been devoted in the last two decades to the investigation of the flow and heat transfer characteristics. The issues of flow stability and bifurcations have been addressed only for long square or rectangular-sectioned cavity with two types of internal source: wires of small diameter and line heat sources [18–21], and horizontal circular or rectangular cylinders [5, 10, 22–25]. In [18] Desrayaud and Lauriat thoroughly investigated the dynamical behaviour of the buoyant plume arising from a horizontal line source, modeled as a point source in a 2D rectangular cavity with adiabatic side walls and isothermal top and bottom walls. The analyses were performed taking air as the heat carrier fluid ($Pr = 0.71$), for several values of the enclosure aspect ratio, and for various depths of immersion of the source along the vertical axis of the cavity. Depending on these two parameters, various dynamics were detected. In particular, for square cavities and moderate depths of immersion, the onset of unsteadiness occurred by the subcritical transition from steady-state to a periodic swaying motion of the buoyant plume. The correspondent route to chaos passed through phase-locking and intermittency states. The progressive increase of the dimensionless dominant frequency appeared to be fairly resolved, thus demonstrating the overall consistency of the results. For higher values of both parameters the scenario changed dramatically. Above the thermal plume, an unstably stratified region was maintained at rest thanks to the hydrostatic gradient, until a pitchfork bifurcation occurred, leading to a non-symmetric bending of the plume, which entrained the above fluid layer. The subsequent transition to oscillatory flow was characterised by hysteresis phenomena, revealing the occurrence of subcritical Hopf bifurcations.

Recently, Angeli et al. [22] investigated by means of 2D finite-volume simulations the nonlinear dynamics of the buoyancy-induced flow of air (Pr=0.7) heated from a horizontal cylindrical source centred in a square enclosure. The study was developed under various geometrical configurations, as defined by the aspect ratio $A = H/L$, i.e. the ratio between the maximum gap height and the length of the side walls. For the cavities with aspect ratio $A = 5$

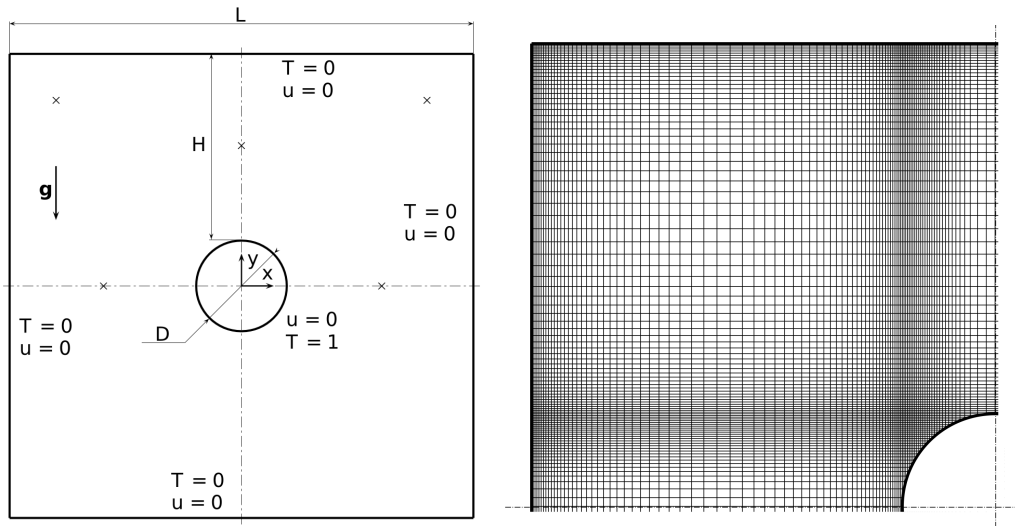

Figure 1. Left: schematic of the system under consideration; (×) symbols indicate locations of the sampling points. Right: quadrant of the computational grid.

and $A = 10$, the flow asset and early bifurcations were found to be primarily determined by the formation of Rayleigh-Benard-type rolls above the heat source. These steady-state, multicellular patterns were seen to undergo symmetry-breaking pitchfork bifurcations, eventually leading to periodic states.For $A = 3.3$ and $A = 2.5$ the dynamics were found to be governed by the oscillations of a swaying thermal plume originating around the cylindrical heat source.

Aiming at an accurate assessment of the entire scenario leading to deterministic chaos, in [26] a single value of the aspect ratio, $A = 2.5$, was analysed in detail adopting a thorough refinement of the range of Ra in order to observe the a sequence of bifurcations leading to chaos. In this study it was shown that the bifurcation scenario can be summarized by a period-doubling route to chaos, originated by a supercritical Hopf bifurcation and followed up to the P_{128} limit cycle. Though this scenario can be considered relatively common for thermofluid dynamic systems, one main peculiarity of the reported bifurcation path is the existence of a window of quasiperiodic behaviour in the range $1.735 \times 10^5 < Ra < 1.790 \times 10^5$, which appears as an imperfect occurrence of the first period doubling, i.e. from a P_1 to a P_2-limit cycle, at the beginning of the mentioned period-doubling cascade. In particular, what appears unusual in the reported scenario is that the disappearance of the quasiperiodic torus corresponds to the birth of a stable P_2 limit cycle and, above all, to the subsequent period doubling cascade. Such a behaviour, atypical for autonomous systems and not yet reported for thermofluid dynamic systems. The aim of the present study is to give further details on the origin, evolution and disappearance of the quasiperiodic T_2-torus mainly through the analyses of the power spectral density distributions and of the topology of the limit cycles and of the torus involved in this restricted sequence of bifurcations.

2. Problem statement

The problem is stated in terms of the incompressible Navier-Stokes formulation. The Oberbeck-Boussinesq approximation is enforced, all the fluid properties being consistently assumed as constant, apart from density in the buoyancy term.

The governing equations are tackled in their non-dimensional form. The gap between the top of the cylinder and the upper cavity wall is indicated in [22] as the most suitable scale length, $H_{ref} = H$. In fact, it reduces the dependence of the solution ranges on the aspect ratio, in particular, for what concerns the heat transfer rate and the first transitions between different

regimes. Moreover, the region above the cylinder is subject to the maximum inverse thermal gradient, *i.e.* to the highest buoyancy force acting on the fluid system, and this is again related to the reference length H.

Temperature is non-dimensionalized according to a reference temperature T_{ref}, *i.e.* the temperature difference between the cylinder and the cavity walls ($T_{ref} = T_S - T_W$), and the following velocity scale is chosen:

$$U_{ref} = \sqrt{g\beta T_{ref} H_{ref}} \tag{1}$$

where g denotes the gravitational acceleration and β is the thermal expansion coefficient of the fluid. The continuity, momentum, and energy equations are given the following form:

$$\nabla \cdot \mathbf{u} = \mathbf{0} \tag{2}$$

$$\frac{\partial \mathbf{u}}{\partial t} + \mathbf{u} \cdot \nabla \mathbf{u} = -\nabla p + \frac{Pr^{1/2}}{Ra^{1/2}} \nabla^2 \mathbf{u} + T\hat{\mathbf{g}} \tag{3}$$

$$\frac{\partial T}{\partial t} + \mathbf{u} \cdot \nabla T = \frac{1}{(RaPr)^{1/2}} \nabla^2 T \tag{4}$$

where t, $\mathbf{u}$, p and T represent the dimensionless time, velocity vector, pressure and temperature, respectively, and $\hat{\mathbf{g}}$ is the gravity unit vector. The Rayleigh and Prandtl numbers are defined as:

$$Ra = \frac{g\beta T_{ref} H_{ref}^3}{\nu\alpha} \tag{5}$$

$$Pr = \nu/\alpha \tag{6}$$

where ν and α represent the momentum and thermal diffusivity, respectively. A constant value $Pr = 0.7$ is assumed for air. With reference to figure 1, the following non-dimensional boundary conditions are imposed:

$$T = 0, \quad \mathbf{u} = \mathbf{0} \tag{7}$$

at the enclosure walls, and:

$$T = 1, \quad \mathbf{u} = \mathbf{0} \tag{8}$$

on the cylinder surface.

3. Numerical methods

The numerical technique adopted is based on a Finite Volume implementation of a second order Projection Method, following [27]. Time-discretizations of the conservation equations are performed according to a three-level scheme, which is fully implicit for the diffusive terms, and explicit Adams-Bashforth for the advective terms. Such a practice is second order accurate in time.

Spatial derivatives are approximated with second order central differences on staggered, non-uniform Cartesian grids. A direct resolution of the discrete momentum and energy equations at each time-step is made possible by means of Approximate Factorization, while the Poisson problem associated with the pressure-velocity coupling [27] is solved through a fast Poisson solver, based on Matrix Decomposition.

The 2D modelling of arbitrarily irregular boundaries on Cartesian grids is achieved thanks to the original scheme developed in [28]. The technique involves a local modification of the 5-point computational stencil where boundary segments intersect the stencil arms. The variables on the modified stencil are mapped on the global grid, by means of a linear operator determined by

geometrical features and boundary conditions. The overall accuracy of the method is virtually preserved, as well as the computational efficiency of the Cartesian approach.

The Cartesian grid employed, made up by 190×190 elements, is shown in figure 1. Along both grid directions, a variable spacing was used, and special care was put on the grid sizing of both near-wall areas and internal domain regions, in view of the work objectives. The criteria adopted for the choice of grid spacing and time step size are outlined in detail in [26], while a grid independency test for a periodic flow is reported in [22].

In order to analyze the system dynamics in the vicinity of bifurcation points, Ra was increased monotonically with suitable steps, each simulation starting from the final frame of the preceeding one. All the simulations were protracted until a fixed dimensionless time span was covered, large enough for an asymptotic flow to be attained [26].

Time histories of dimensionless temperature T, and velocity components along x and y directions, respectively u_x and u_y, were tracked for 5 locations, reported in figure 1, and analysed by means of classical tools for nonlinear time series analysis, such as phase-space representations, power spectra and Poincaré maps.

4. Results and discussion

In the present section, the dynamical behaviour of the system under investigation is described for the cavity of aspect ratio A = 2.5, characterized by a thermal plume whose swaying motion is dependent on the intensity of the buoyancy force, i.e. on the forcing term Ra [29]. Reported results refer to the system variables simulated at point (0; 0.5) and are representative of the dynamics observed in the other points. In particular, the dynamics in the other control points are equivalent, in terms of both spectral analysis and phase-space topology, to those described in the following.

For increasing values of the Rayleigh number, the adoption of an accurate scanning of the bifurcation parameter allowed the observation of the entire sequence of bifurcations driving the plume from stationary to chaotic motion as summarized in table 1 and discussed in detail by Angeli and Pagano [26]. From the analysis of table 1 it clearly emerges that the bifurcation scenario is, in general, well described by a Feigenbaum cascade. In other terms, for increasing Ra-values the periodicity of the plume oscillation undergoes a series of doublings, which occur closer and closer to one another until chaos appears. Nonetheless, it is worth observing that this paradigm appears distorted by the occurrence, at the beginning of the period doubling, of a window of Ra-values characterized by the quasiperiodic oscillation of the thermal plume. In

Table 1. Flow regimes and corresponding ranges of Ra throughout the transition to chaos [26].

flow regime		$Ra \times 10^{-5}$
steady-state	S	≤ 0.66200
periodic	P_1	$0.66200 \div 1.73500$
quasiperiodic	QP	$1.74000 \div 1.79270$
periodic	P_2	$1.79280 \div 1.89750$
periodic	P_4	$1.89800 \div 1.93670$
periodic	P_8	$1.93675 \div 1.94730$
periodic	P_{16}	$1.94735 \div 1.94950$
periodic	P_{32}	$1.94955 \div 1.94990$
periodic	P_{64}	$1.94995 \div 1.95002$
periodic	P_{128}	$1.95002 \div 1.95010$
chaos	N	≥ 1.95025

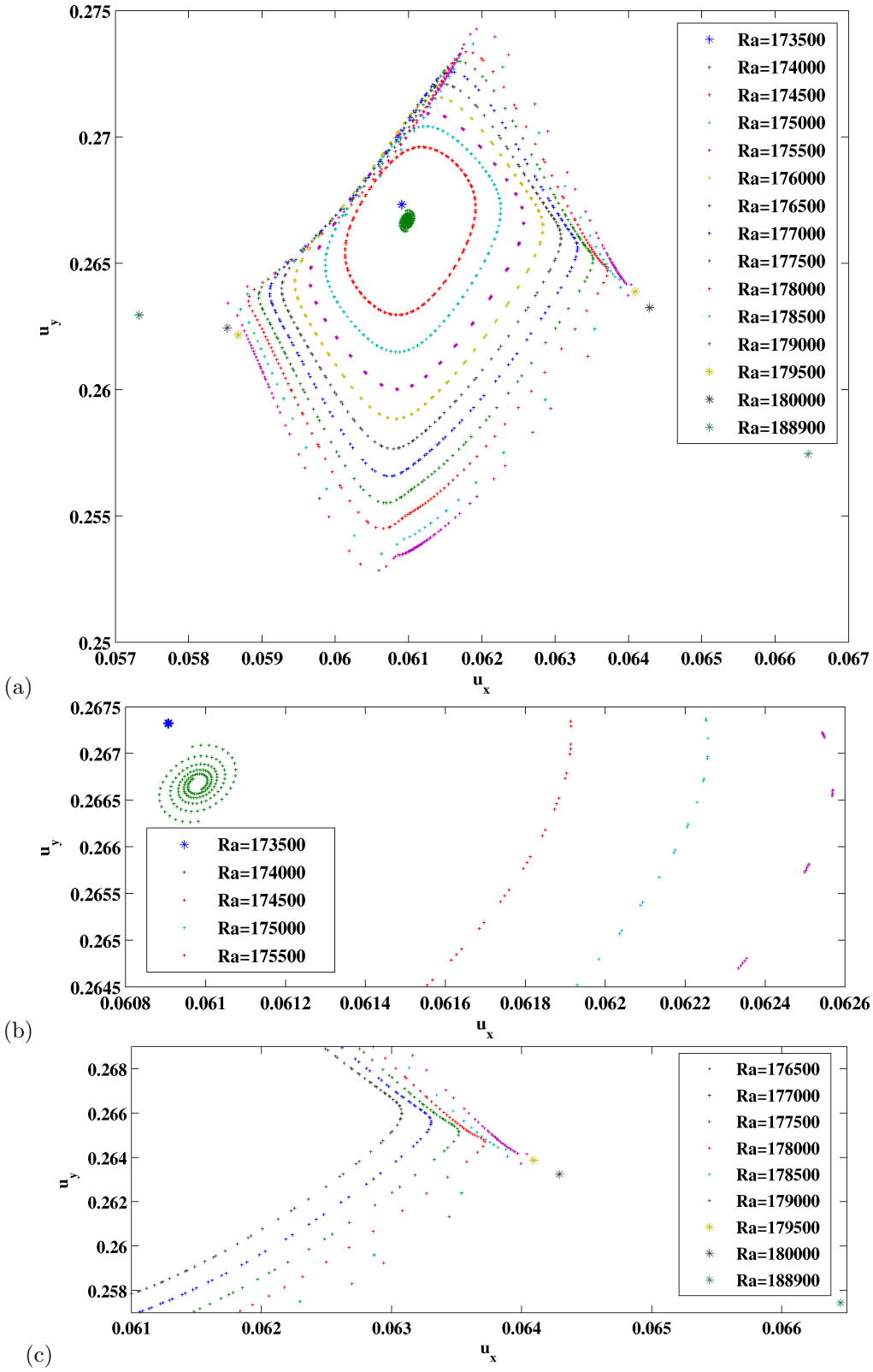

Figure 2. Sequence of Poincaré maps at point (0; 0.5) (a) spanning the whole range of Ra considered; (b) enlarged view of the $P_1 \rightarrow QP_2$ transition range; (c) enlarged view of the $QP_2 \rightarrow P_2$ transition range.

this contest, the present study aims at offering a deeper insight on the plume dynamics within the window of quasiperiodic dynamics and in its immediate neighborhoods.

As it is shown in table 1, for $Ra \geq 1.735 \times 10^5$ the formerly stable P_1 limit cycle becomes unstable. In fact, a new attractor of the system dynamics appears in phase space in the shape of a dense T_2 torus, typical of quasiperiodic dynamics characterised by two incommensurate frequencies. The bifurcation of the P_1 limit cycle to the T_2 torus implies the occurrence of a Neimark-Sacker bifurcation [30]. Considering that the classical Feigenbaum doubling scenario is determined by a series of flip bifurcations of limit cycles [30], the reported observation implies that the first of these bifurcations is replaced by a Neimark-Sacker bifurcation followed by the collapse of the T_2 torus onto a P_2 limit cycle. The Neimark-Sacker bifurcation leads to the permanence of the unstable P_1 limit cycle in the wake of a ghost entrapped inside the torus and acting as an axis for it.

A clear documentation of this behavior is represented by the evolution of the topology of the Poincaré maps of the T_2 torus reported in figure 2a and in its local detail reported in figure 2b. The Poincaré sections were obtained by cutting the attractors with the secant plane normal to the T-coordinate, at its mean value. The exact location of the intersections was determined by linear interpolation of the position of two points on the opposite sides of the secant plane. The interpolation error is negligible due to the high resolution of the simulated time series. From the analysis of these figures, in fact, it emerges that all of the pseudo-elliptic maps, i.e. the characteristic traces of T_2 tori onto the Poincaré surface of section, are centered on the stationary point, marginally stable, of the map at $Ra = 173500$. As a consequence, one main consideration that can be drawn is that, referring to the torus axis, only marginal variations occur with the increase of the Rayleigh number, i.e. the torus amplitude and its general topology in phase space are not sensitively altered. In fact, the most important influence of the growing energy associated to the increase of Ra within the range of quasiperiodic behavior is indeed represented by the progressive enlargement of the torus trace onto the Poincaré plane. In other terms, the higher is the value of the forcing term, Ra, the larger is the torus trace, which, in turn, is associated to the relative importance of the second incommensurate frequency with respect to the primary one, inherited from the unstable limit cycle and associated to the dominant feature of the motion around the torus axis.

At the same time, another important effect associated to the increase of Ra is the progressive deformation of the transversal section of the torus. In particular, the Poincaré section, while remaining dense, progressively changes its shape. From the analysis of the general behavior in figure 2 and of the specific behaviors at $Ra = 174500$ in figure 3 and at $Ra = 178500$ in figure 4, it is possible to observe that the pseudo-elliptical shape, which is a typical feature of a Poincaré traces at the onset of the quasiperiodic dynamics on a torus, is progressively deformed, eventually turning into a pseudo-rectangle, with a marked local deformation of its edges. Moreover, the edges of the pseudo-rectangular Poincaré trace assume the behavior of saddle points on the Poincar map (see figure 2c and 4c-e). From the plots, the progressive and relatively slow accumulation of the traces of the trajectory approaching them on one direction and the abrupt repelling action on the direction pseudo-orthogonal to the first appear evidently. It is then possible to explain the disappearance of the torus and the birth of the P_2 limit cycle as a consequence of the destruction of a couple of opposite edges of the pseudorectangular Poincaré trace, and of the stabilization of the remaining couple of saddles, i.e. of the two branches of the stable P_2 limit cycle on the 3D state space.

Some further details, substantially confirming the description reported so far on the topology of the T_2 torus in the 3D state space and of its Poincaré section in 2D, can be drawn from the analysis in the frequency domain. As it was shown in [26], within the range of quasiperiodic behavior, two incommensurate frequencies f_1 and f_2 exist, which are only marginally influenced by the value of Ra, and so it happens to their ratio, f_2/f_1. The main effect of the increase

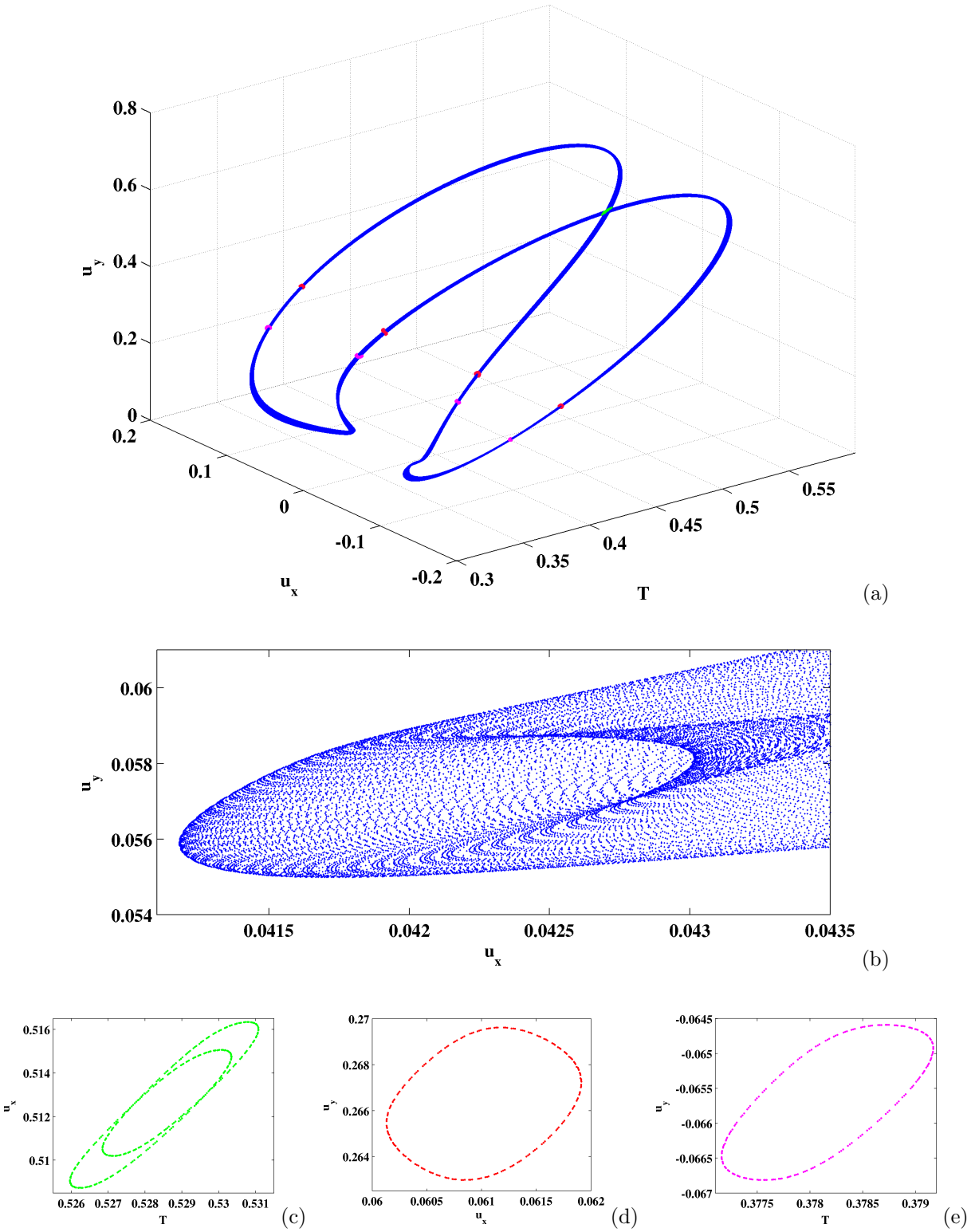

Figure 3. Phase plots of the quasiperiodic dynamical behaviour at point (0; 0.5) for $Ra = 174500$: (a) attractor in the state space T-u_x-u_y; (b) particular evidencing the structure of the T_2 torus; (c), (d), (e) Poincaré maps.

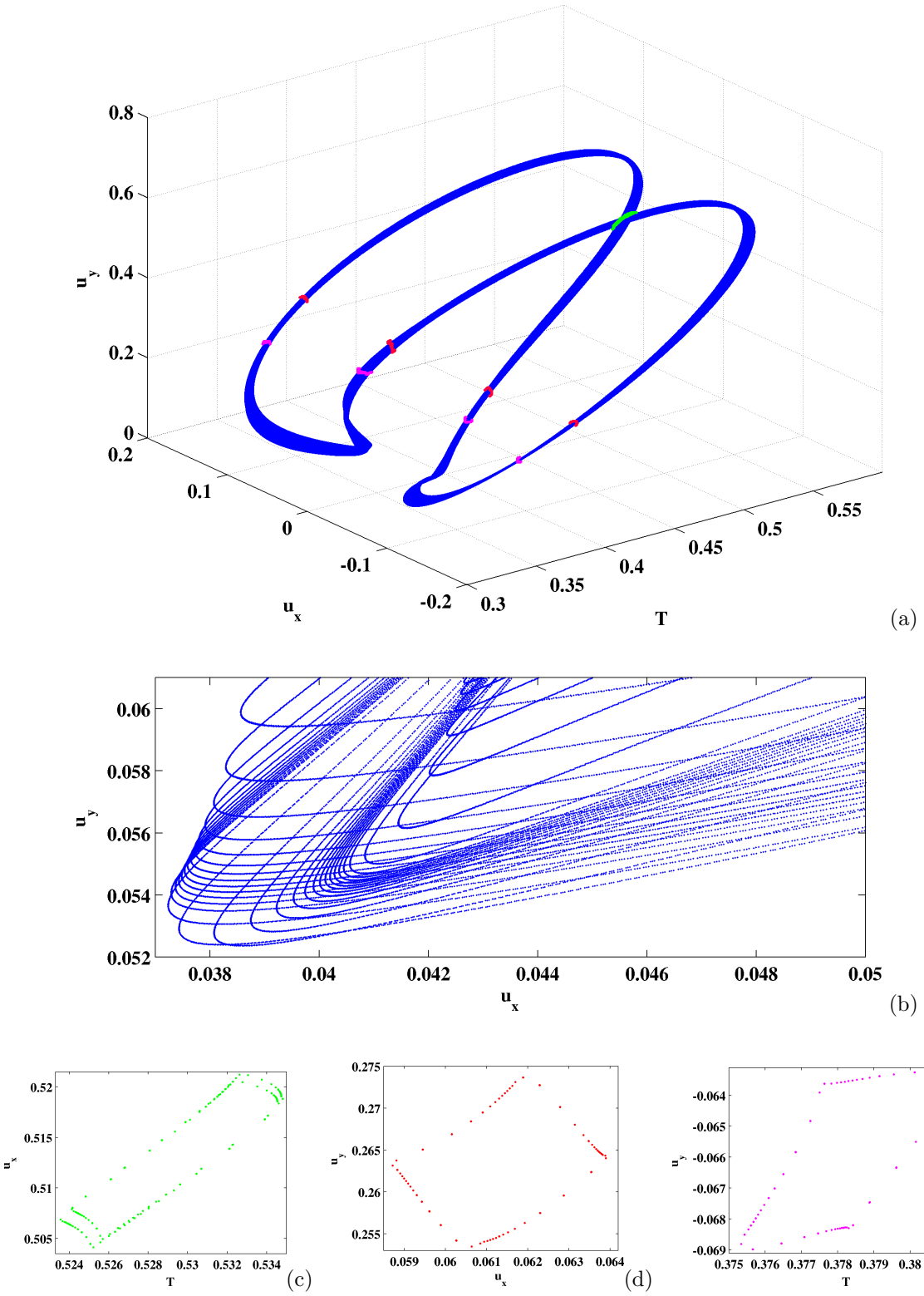

Figure 4. Phase plots of the quasiperiodic dynamical behaviour at point (0; 0.5) for $Ra = 178500$: (a) attractor in the state space T-u_x-u_y; (b) particular evidencing the structure of the T_2 torus; (c), (d), (e) Poincaré maps.

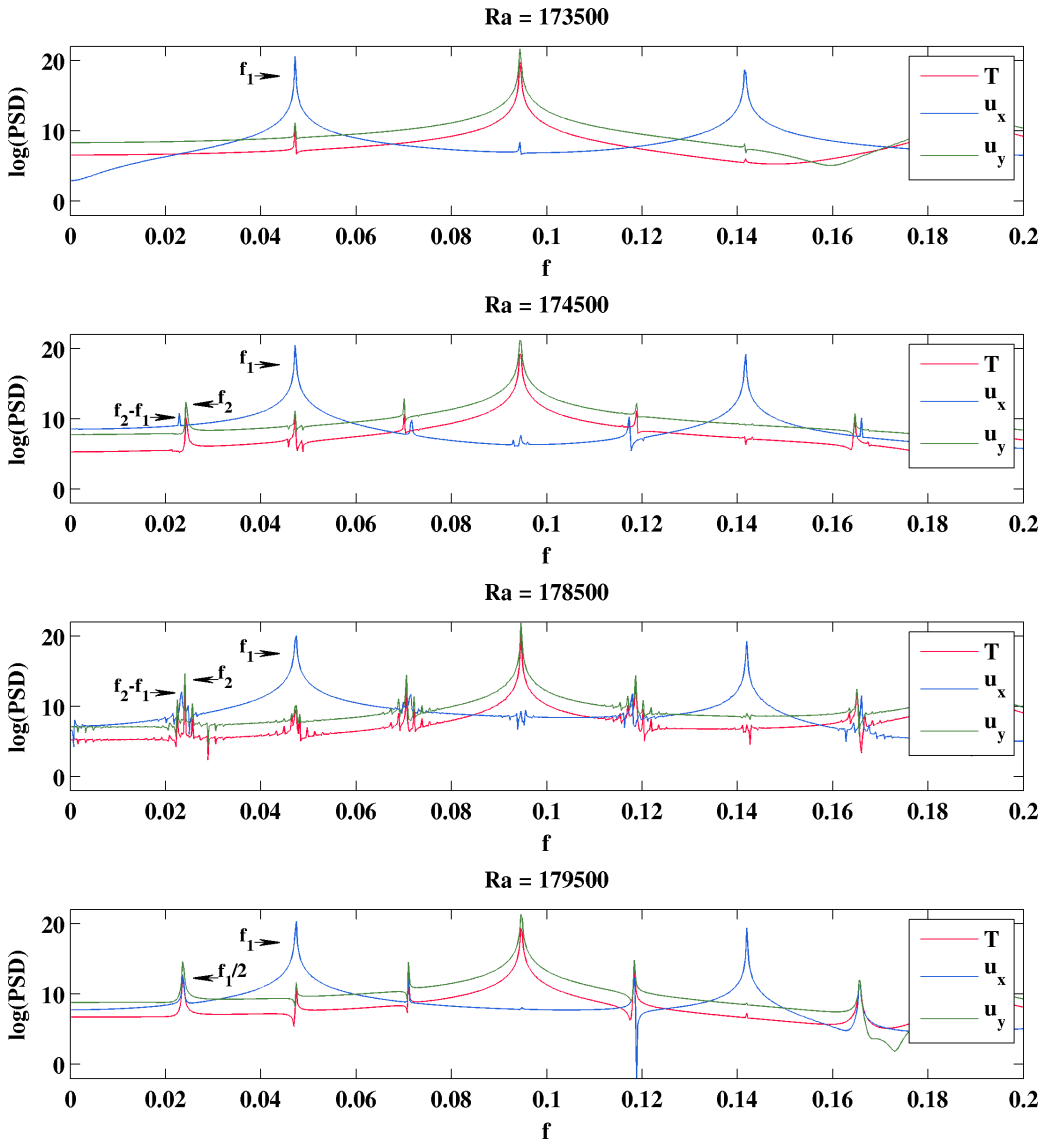

Figure 5. PSD distribution of T, u_x and u_y at point (0;0.5) for selected Ra-values

of Ra on the power spectral density (PSD) can be drawn from the analysis of figure 5. In accordance with previous observations on the progressive enlargement of the Poincaré traces, it can be observed that the power associated to the secondary frequency, f_2, and to its harmonic combinations with f_1, clearly increases with Ra. The analysis of the PSD also helps to stress the nature of imperfect period doubling, i.e. of the missed flip bifurcation of the P_1 limit cycle, that gives rise to the reported Neimark-Sacker bifurcation. In fact, within the entire range of quasiperiodic behavior:

- the secondary frequency f_2 is always very close to $f_1/2$;
- the main harmonic combination of f_1 and f_2 emerging in the PSD for all of the simulated time series is always the frequency $f = f_1 - f_2$;
- the amplitude of $f = f_1 - f_2$ is comparable with that of f_2, and, for increasing Ra, further harmonic combinations of the two main frequencies arise in the PSD
- accordingly, the trajectories distribute themselves onto the T_2-torus through an almost

parallel and alternated winding on opposite sides of the torus itself.

As a final observation, it is worth noting that, for increasing Ra, the difference between f_2 and the harmonic $f_1 - f_2$ progressively decreases, until they collide for $Ra = 1.7928 \times 10^5$, leading to the disappearance of the quasiperiodic torus and to the birth of a stable P_2 limit cycle, as reported in figure 2a and 2c.

5. Concluding remarks

The occurrence of quasiperiodicity preluding a sequence of period-doubling bifurcations leading to deterministic chaos was analysed in detail by numerical means, for a natural convection flow originating from a horizontal cylindrical source, centred in a square enclosure of aspect ratio $A = 2.5$.

The analysis of long-term, highly resolved time series, extracted from numerical predictions of the asymptotic system behaviour, allowed for the disclosure of significant features of such a peculiar bifurcation pattern. The quasiperiodic orbit originates from the destabilization of a P_1 periodic orbit, through a Neimark-Sacker bifurcation, and then disappears giving way to a second periodic orbit P_2, whose fundamental frequency is equal to half of the frequency of the P_1 orbit. The topological evolution of the T_2 torus in the 3D state space, and of the related traces in the Poincaré maps, revealed the progressive creation of singularities in the shape of the attractor, in the form of four accumulation curves, corresponding, in the Poincaré section, to the four corners of a pseudorectangle. Eventually, two of such singularities disappear, while the remaining two survive in the P_2 orbit. Furthermore, the analysis of the time series in the frequency domain indicate that the halving of the fundamental frequency f_1 of the P_1 orbit results from the collision between the secondary frequency f_2 of the quasiperiodic flow and the harmonic $f_1 - f_2$.

The observed behaviour suggests that, in the present case, the Neimark-Sacker bifurcation replaces the first flip bifurcation of a classical Feigenbaum sequence, and may then be viewed as an imperfect period doubling, a feature yet unprecedented in confined convective flows.

References

[1] Yang K T 1988 *J. Heat. Transf.* **110** 1191–1204
[2] Le Quéré P 1994 *Procs. 10th Int. Heat Transf. Conf.* vol 1 ed Hewitt G F (Brighton, UK: Hemisphere Publishing Corporation) pp 281–296
[3] Angeli D, Barozzi G S, Collins M W and Kamiyo O M 2010 *Int. J. Therm. Sci.* **49** 2231–2492
[4] Warrington J R O and Powe R E 1985 *Int. J. Heat Mass Transf.* **28** 319–330
[5] Cesini G, Paroncini M, Cortella G and Manzan M 1999 *Int. J. Heat Mass Transf.* **42** 1801–1811
[6] Kim B S, Lee D S, Ha M Y and Yoon H S 2008 *Int. J. Heat Mass Transf.* **51** 1888–1906
[7] Lee J M, Ha M Y and Yoon H S 2010 *Int. J. Heat Mass Transf.* **53** 5905 – 5919
[8] Paroncini M and Corvaro F 2009 *Int. J. Therm. Sci.* **48** 1683–1695
[9] Butler C, Newport D and Geron M 2012 *Exper. Therm. Fluid Sci.* Article in press
[10] Peng Y, Chew Y T and Shu C 2004 *Phys. Rev. E* **67** 026701/1–026701/6
[11] Bararnia H, Soleimani S and Ganji D D 2011 *Int. Comm. Heat Mass Transf.* **38** 1436 – 1442
[12] Nabavizadeh S A, Talebi S, Sefid M and Nourmohammadzadeh M 2012 *Int. J. Therm. Sci.* **51** 112 – 120
[13] Bergé P, Pomeau Y and Vidal C 1988 *L'Ordre dans le Chaos* 2nd ed (Hermann, Editeurs des Sciences et des Arts)
[14] Gollub J P and Benson S V 1980 *J. Fluid Mech.* **100** 449–470
[15] Yoo J S, Choi J Y and Kim M U 1994 *Num. Heat Transf. A* **25** 103–115
[16] Yoo J S and Han S M 2000 *Fluid Dyn. Res.* **27** 231–245
[17] Labonia G and Guj G 1998 *J. Fluid Mech.* **375** 179–202
[18] Desrayaud G and Lauriat G 1998 *J. Fluid Mech.* **252** 617–646
[19] Deschamps V and Desrayaud G 1994 *J. Thermophys. Heat Transf.* **8** 84–91
[20] Lauriat G and Desrayaud G 1994 *Sādhanā* **19** 671–703
[21] Barozzi G S and Corticelli M A 1999 *Procs. 6th* UK *Nat. Conf. Heat Transf.* (IM*ech*E *Conference Transactions* vol 1) ed Hahane E W P, Heidemann W and Spindler K (Edimburgh, UK: Professional Engineering Publishings) pp 69–74

[22] Angeli D, Levoni P and Barozzi G S 2008 *Int. J. Heat Mass Transf.* **51** 553–565
[23] Ghaddar N K 1992 *Int. J. Heat Mass Transf.* **35** 2327–2334
[24] Moukalled F and Acharya S 1996 *Journal of Thermophys.* **10** 524–531
[25] Shu C and Zhu Y D 2002 *Int. J. Num. Meth. Fluids* **38** 429–445
[26] Angeli D and Pagano A 2013 *Int. J. Therm. Sci.* **68** 20–31
[27] Gresho P M 1990 *Int. J. Num. Meth. Fluids* **11** 587–620
[28] Barozzi G S, Bussi C and Corticelli M A 2004 *Numerical Heat Transfer B* **46** 56–77
[29] Bouafia M and Daube O 2007 *Int. J. Heat Mass Transf.* **50** 3599–3615
[30] Kuznetsov Y 1998 *Elements of Applied Bifurcation Theory* 2nd ed (*Applied Mathematical Sciences* vol 112) (New York: Springer-Verlag)